Analysis of the Eddy-Current Induced Artifacts and the Temporal Compensation in Nuclear Magnetic Resonance Imaging

C. B. Ahn, *Member, IEEE,* and Z. H. Cho, *Fellow, IEEE*

Abstract—Effects of eddy currents in nuclear magnetic resonance imaging (NMR) are investigated from the solution of Maxwell's equations. The point spread functions affected by the eddy currents appear broader and shifted, resulting in resolution degradation as well as misregisteration. The intensity and phase variations caused by the eddy currents can also generate problems associated with intensity and phase-sensitive imaging techniques. In this paper, reduction of eddy currents by a temporal compensation of the input current waveform to the gradient coil is studied with analytic solution. The limitation of the temporal compensation due to the spatially variant eddy currents is also investigated for both whole body diagnostic imaging system and small bore NMR microscopy system. Within a limited imaging volume of less than 60% of the gradient coil diameter, it appeared that most of eddy current problems can be solved by the temporal compensation technique.

I. Introduction

A NALYSIS of eddy currents in nuclear magnetic resonance imaging has been recently carried out from a solution of Maxwell's equations [1]-[2]. As will be shown later in this paper, eddy currents introduce resolution degradation, misregisteration, and intensity and phase variations.

Most of eddy-current compensation techniques developed can be classified into two categories, i.e., temporal compensation of the input current waveform to the gradient coil [3]-[5] and self-shielded gradient coil approach [6]-[7]. The former is to modify the input current waveform to the gradient coil in time domain in such a way that the resultant gradient field would be closer to the desirable response, while the latter is to design a gradient coil which generates not only a linear gradient field inside of the coil but also a null field outside of the coil thereby eliminating interactions between gradient coil and magnet. The temporal approach is relatively simple to implement; however, accurate compensation in overall imaging volume is limited due to space-variant characteristics of eddy currents. On the other hand, the space-variant eddy currents can be corrected by the self-shielded gradient coil with a proper design of two-dimensional multiple shielding layers. However, this approach requires rebuilding whole gradient coil set for existing nonshielded gradient coil system.

Although "eddy currents" is one of the most familiar terms in NMR imaging and the temporal compensation technique is nothing new [3]-[5], few studies have been carried out systematically about eddy-current induced image artifact and accuracy of the compensation by temporal techniques. In this paper, investigations are focused on the characteristics of eddy-current induced artifacts and compensation by the temporal approach. Limitation of the temporal compensation technique due to space-variant eddy currents will be evaluated with the analytic formula.

II. Effects of Eddy Currents in NMR Imaging

In order to investigate effects of eddy currents in NMR imaging, a brief review of the analytic solution of the eddy currents would be necessary. The vector potential A satisfying the diffusion equation [8]-[9] can be written in NMR imaging system as

$$\nabla^2 A_I = 0, \quad \rho \leq R$$
$$\nabla^2 A_{II} = \mu\sigma \frac{\partial A_{II}}{\partial t}, \quad \rho > R \qquad (1)$$

where R is the radius of the magnet in the cylindrical coordinate (ρ, φ, z), and μ and σ are the permeability and conductivity of the magnet wall, respectively. By solving (1), the magnetic induction or magnetic field in imaging region $(\rho \leq r)$ is given for a unit current loop with a time-dependent term of $e^{i\omega t}$ by

$$B^z(\rho, z, \omega) = (\nabla \times A_I)_z$$
$$= \frac{1}{\rho} \frac{\partial}{\partial \rho} (\rho A_I^\varphi)$$
$$= \frac{\mu r}{\pi} \int_0^\infty k I_0(k\rho) K_1(kr) \cos(kz) dk$$
$$+ \int_0^\infty C(k, \omega) k I_0(k\rho) \cos(kz) dk \qquad (2)$$

where r is the radius of the gradient coil $(r < R)$, B^z is the z-component of B with the magnet bore assumed to be in parallel to the z axis, and A^φ is the φ-component of A. In (2), $I_n(\cdot)$ and $K_n(\cdot)$ are the nth-order modified Bessel functions, and $C(k, \omega)$ is determined from boundary conditions as

$$C(k, \omega) = \frac{\mu r I_1(kr) \left[k K_0(kR) K_1(\eta R) - \eta K_1(kR) K_0(\eta R) \right]}{\pi \left[\eta K_0(\eta R) I_1(kR) + k I_0(kR) K_1(\eta R) \right]}$$

$$(3)$$

where $\eta^2 = k^2 + i\omega\mu\sigma$. In deriving (1)-(3), magnet is assumed to have an infinite wall-thickness and longitudinal length and the current loop is located at the center of the magnet. In order to obtain the field response in time domain, (2) is further trans-

formed as

$$b^z(\rho, z, t) = \frac{1}{2\pi} \int_{-\infty}^{\infty} B^z(\rho, z, \omega) G_z(\omega) \exp(i\omega t) \, d\omega \quad (4)$$

where $G_z(\omega)$ is the Fourier transform of the input current waveform. The magnetic induction within a gradient coil may be obtained by a proper superposition of the magnetic field in (2). For example, if a Maxwell pair is employed for a z gradient, then the magnetic induction inside of the gradient coil becomes $b_g^z(\rho, z, t) = b^z(\rho, z - z_0, t) - b^z(\rho, z + z_0, t)$, with $z_0 = 0.866r$ for an optimal gradient field linearity. Although a real magnetic resonance imaging (MRI) system is much more complicated than the model used, the simple model may be applicable to the study of eddy current effects and the performance analysis of the temporal compensation.

In order to investigate eddy current effects in NMR imaging, magnetic inductions inside of the Maxwell pair ($\rho = 0$, $z = 0.2r$ from the center of the gradient coil) are numerically evaluated using (2) and (4) for a rectangular current input. Fig. 1(a) shows the field response when the gradient coil is placed outside of the magnet and Fig. 1(c) shows the field response when the gradient coil is located inside of the magnet. The magnet bore diameter and the gradient coil diameter are 7 and 5.6cm, respectively, for simulation of a microscopy system [10]-[11]. Simulated free induction decay (FID) signals for a period of 8.5ms (256 point sampling with a sampling interval of 33μs), starting 0.2ms after the application of the gradient field, are also shown in Fig. 1(b) and (d) for a point source located at $z = 0.2r$. Note the varying frequencies observed in (d), especially at the beginning of the data acquisition period, in contrast to the monoenergetic sinusoidal function in (b).

Results of the Fourier transform of the simulated NMR signals are shown in Fig. 2. A sinc function centered at $z = 0.2$ r (location of the point object) is obtained for real part (a) and negligible intensities for imaginary part (c) in the case of the signal under free from eddy currents. The impulse response under the eddy currents shown in Fig. 2(b), (d), and (f) is, however, quite different from the ideal response with several distinct distortions: i) split peaks instead of single peak as observed in Fig. 2(b) due to varying frequencies, ii) peak location shift, iii) intensity attenuation as observed in Fig. 2(f) compared to Fig. 2(e) due to line broadening, and iv) phase change at peak location. The split peak can generate multiple edges in the reconstructed image as well as resolution degradation. Misregisteration caused by the eddy currents is often observed in the multiply acquired images with different experimental parameters. For example, 1 or 2 pixel shifts are easily observed in the images obtained with different repetition times, thereby different eddy current effects, in the calculation of a T_1 map. The intensity attenuation and phase variation not only bring a reduction of signal-to-noise ratio but also cause serious problems associated with intensity and phase-sensitive imaging techniques such as diffusion, perfusion, and MR angiography [12]-[14]. These distortions are numerically evaluated in Table I as a function of the spatial coordinate. As shown in this table, degradations of the impulse response by the eddy currents are serious. For example, the full width at half maximum ($fwhm$) in the plane, $z = 0.6r$, is more than 5 times larger than that of sinc function. Note that the $fwhm$ is increasing as object location moves farther from the center. This is due to the increase
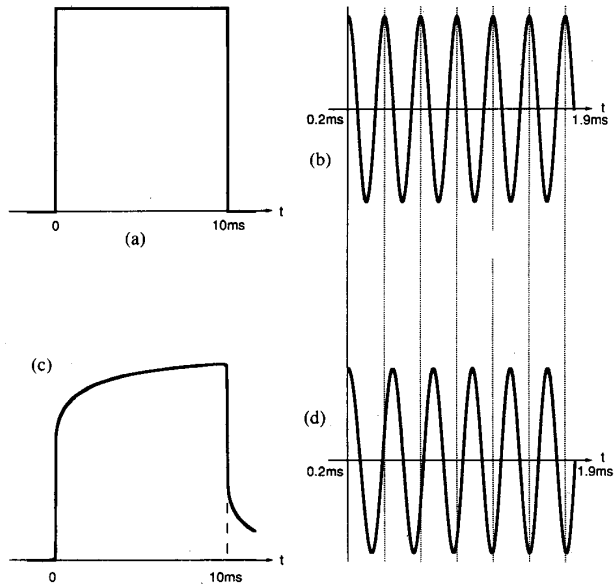

Fig. 1. Two magnetic inductions and corresponding NMR signals are numerically calculated for a rectangular current input. (a) Magnetic induction free from eddy currents (flat during data acquisition). (b) A part of NMR signal ($\sim 1/5$ of the acquisition period) calculated with the magnetic induction in (a) is shown after demodulation (only real part of the signal is shown). Since the phase is linearly increasing, the signal is a cosine function. (c) Magnetic induction affected by the eddy currents. (d) The NMR signal with the magnetic induction in (c). Note the varying frequencies or changing peak-to-peak distances in the signal.

of eddy-current induced field as a function of z (there is no field distortion in $z = 0$ plane due to the symmetric geometry of the Maxwell pair). Although the field intensity produced by external currents is also linearly increasing as a function of z inside of the gradient coil, the amount of distortion in spin phase is proportional to the absolute amplitude of the eddy-current induced field rather than the ratio of the induced field to the generated field. For example, if a delta function is placed at $z = 5$ Δz with pixel size Δz, and if 10% of frequency variation is introduced by the eddy currents, then the spatial variation ($fwhm$) after the Fourier transform is about 0.5 Δz. However, if a delta function is located at $z = 100$ Δz, the spatial variation would be 10 Δz for the same frequency variation. The shift of peak position appears as much as 1-2 pixels, depending on the spatial location of the object. The space-dependent intensity attenuation is more than 50%, and the peak-phase variation by the eddy currents is more than 100° in some cases (e.g., $z = 0.8r$, $\rho = 0.2r$). Spatially varying eddy-current-induced-field map may be obtained by imaging technique in [15].

III. TEMPORAL COMPENSATION OF EDDY CURRENTS

The temporal compensation of the eddy currents in Fourier imaging is to design an input current waveform to the gradient coil in such a way that the variation of the gradient field during the data acquisition period becomes minimum with a minimum transient time. From (4), compensated waveform $\hat{g}_z(t)$ can be
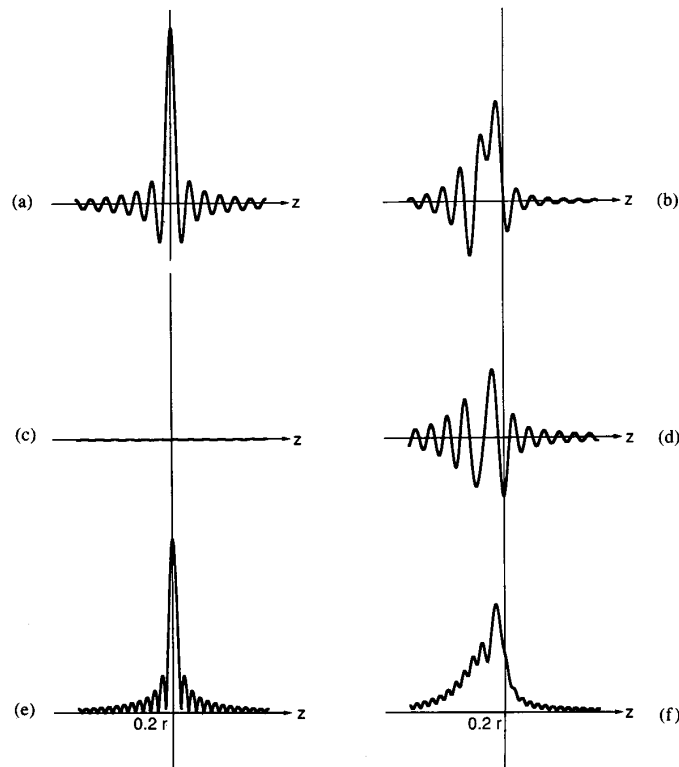
Fig. 2. Two impulse responses with and without eddy currents are plotted by the Fourier transform of the NMR signals shown in Fig. 1. The response without eddy currents is shown in (a), (c), and (e) in the order of real, imaginary, and magnitude. The response under the eddy currents is also shown in (b), (d), and (f) in the same order. All these plots are shown in the same scale.

TABLE I

EDDY CURRENT EFFECTS ARE NUMERICALLY EVALUATED FROM THE SIMULATED NMR SIGNAL AT VARIOUS LOCATIONS (ρ, z DENOTE THE LOCATION OF THE POINT SOURCE) COVERING OVERALL IMAGING VOLUME WITH FOUR PARAMETERS: i) FULL WIDTH AT HALF MAXIMUM OF THE MAIN LOBE NORMALIZED WITH THAT OF THE SINC FUNCTION, ii) SHIFT OF PEAK LOCATION, iii) NORMALIZED PEAK INTENSITY WITH SINC FUNCTION, AND iv) PEAK PHASE.

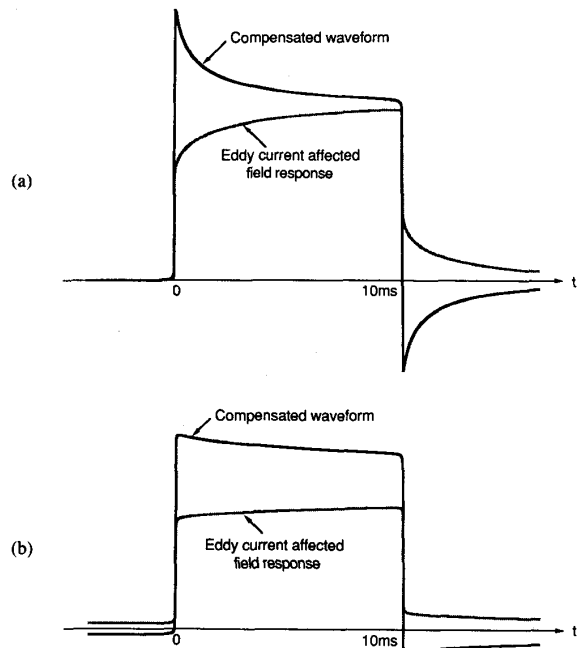|		$\rho = 0$	$\rho = 0.2r$	$\rho = 0.4r$	$\rho = 0.6r$	$\rho = 0.8r$
	Fwhm	1.94	1.95	2.00	3.30	3.88
$z = 0.2r$	Shift (pixel)	-1.09	-1.13	-1.25	-1.22	-1.69
	Intensity	0.61	0.60	0.57	0.52	0.44
	Phase (degree)	23.7	23.0	18.8	-2.70	17.7
	Fwhm	4.93	4.95	4.99	4.07	6.12
$z = 0.4r$	Shift (pixel)	-1.56	-1.50	-1.47	-1.84	-2.25
	Intensity	0.44	0.44	0.43	0.44	0.37
	Phase (degree)	34.9	34.2	29.3	11.2	-77.3
	Fwhm	5.61	5.56	5.47	5.43	5.90
$z = 0.6r$	Shift (pixel)	-1.97	-1.94	-1.88	-1.84	-1.91
	Intensity	0.41	0.41	0.42	0.42	0.39
	Phase (degree)	-30.9	-28.8	-23.5	-19.8	-54.5
	Fwhm	7.68	7.64	6.26	6.92	3.90
$z = 0.8r$	Shift (pixel)	-2.16	-2.06	-2.31	-2.03	-1.69
	Intensity	0.36	0.36	0.37	0.39	0.44
	Phase (degree)	-121.7	-115.0	-90.1	-46.3	19.1

Fig. 3. The compensated waveforms obtained by the inverse filtering of the eddy-current affected fields are shown for a small bore system (a) and for a large bore system (b). The field responses affected by the eddy currents are also shown in shaded lines for references.

obtained as

$$\hat{g}_z(t) = \frac{1}{2\pi} \int_{-\infty}^{\infty} \frac{G_z(\omega)}{B_g^z(\rho, z, \omega)} \exp\left(i\omega t\right) d\omega \qquad (5)$$

where $B_g^z(\rho, z, \omega)$ represents the frequency response of the magnetic induction inside of the gradient coil, and $G_z(\omega)$ is the frequency response of the desirable magnetic field. Using (5), two compensated waveforms are evaluated and are shown in Fig. 3 for Maxwell pairs in a small bore system (a) and in a large bore system (b). The magnet bore diameters are 7 and 80cm, respectively, for the simluation of microscopy and whole body diagnostic systems. The diameters of the gradient coils are assumed to be 80% of the magnet bore diameters. Since the two field responses affected by the eddy currents are quite different, the compensated waveforms are also different, i.e., more high frequency components are employed for the compensated waveform in the small bore microscopy system corresponding to high-frequency related distortions, while low-frequency related compensation is applied to the large bore system. This is due to the fact that the low frequency cutoff is inversely proportional to the square of the magnet bore diameter as discussed in [1]. The results of the temporal compensation are shown in Figs. 4 and 5 for the respective small bore and large bore systems used in the previous examples. The field responses at $z = 0.4r$ and $\rho = 0.2r$ are shown in Figs. 4(a) and 5(a) with the compensated waveforms derived from the eddy-current affected field responses at $z = 0.2r$ and $\rho = 0$. Note the different locations chosen for the derivation of compensated waveform and the calculation of the field response to see mismatching effects. The corresponding impulse responses are plotted in Figs. 4(b) and 5(b). The field and impulse responses with uncompensated
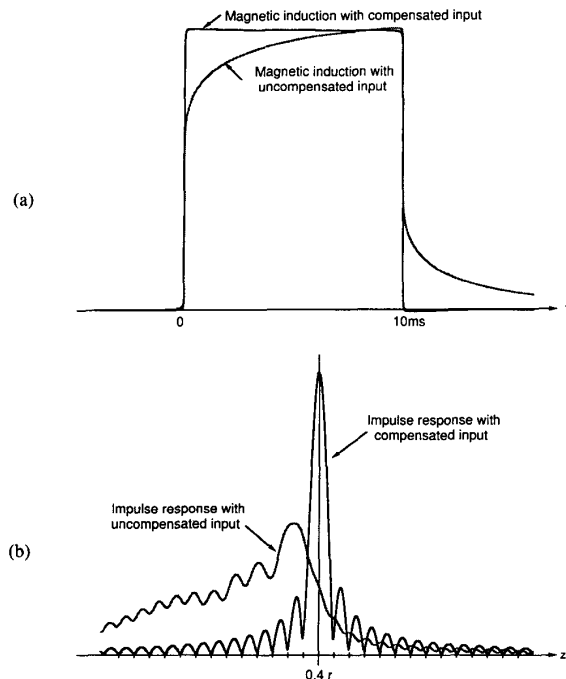

Fig. 4. The magnetic induction and the impulse response calculated at $z = 0.4r$ and $\rho = 0.2r$ in the small bore system are shown with the compensated waveform derived from the eddy-current affected field response at $z = 0.2r$ and $\rho = 0$. The magnetic induction and the impulse response with the uncompensated rectangular input are also shown in shaded lines for references.

rectangular input current are also shown in shaded lines for references. As shown in these figures, the field responses with the compensated input waveforms are very close to the ideal rectangular functions, only with slight tilts during the data acquisition periods due to the mismatching of the compensated waveforms to the eddy currents. The impulse responses are also almost identical to the sinc function except small asymmetries in side lobes. Once the compensated waveform is obtained, it is stored in the waveform synthesizer and is applied repeatedly without hardware addition or modification [5].

As shown in previous examples in Figs. 4 and 5, the performances of the temporal compensation are dependent on the deviations of the compensated waveform to the spatially variant eddy currents. In order to see spatially varying mismatching effects, the *fwhms* of the impulse responses at various locations are evaluated in Table II for the compensated waveforms used in Figs. 4 and 5. From Table II, mismatching effects appear relatively small for a central imaging volume of within 60% of the gradient coil diameter, where the average *fwhms* are 1.06 (largest 1.27) and 1.01 (largest 1.03) for the microscopy system and the whole body system, respectively. The mismatching effects in larger imaging volume (80% of the gradient coil diameter), however, become larger, i.e., the average *fwhms* are 1.41 and 1.44 for the respective microscopy system and whole body system. Although there are considerable mismatching effects near the gradient coil boundary, the improvements by the temporal compensation are substantial. For example, the average *fwhm* for the microscopy system without compensation is 3.73 in the imaging volume of 60% of the gradient coil diameter, and 4.48 in the imaging volume of 80% of the gradient
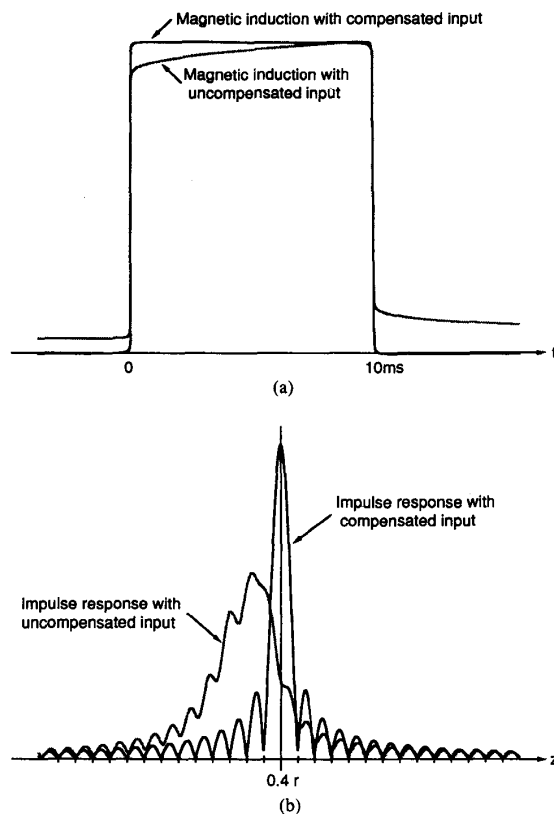
Fig. 5. The magnetic induction and the impulse response calculated at $z = 0.4r$ and $\rho = 0.2r$ in the large bore system are shown with the compensated waveform derived from the eddy-current affected field response at $z = 0.2r$ and $\rho = 0$. The magnetic induction and the impulse response with the uncompensated rectangular input are also shown in shaded lines for references.

TABLE II

Fwhms OF THE IMPULSE RESPONSE FOR THE COMPENSATED INPUT CURRENT WAVEFORMS. THE NUMBER IN THE UPPER ROW IS THE *fwhms* IN THE SMALL BORE SYSTEM AND THE NUMBER IN THE LOWER PARENTHESIS DENOTES THE *fwhms* IN THE LARGE BORE SYSTEM. ALL THE SIMULATION CONDITIONS ARE THE SAME AS IN TABLE I, EXCEPT THE INCLUSION OF THE TEMPORAL COMPENSATION.

	$\rho = 0$	$\rho = 0.2r$	$\rho = 0.4r$	$\rho = 0.6r$	$\rho = 0.8r$
$z = 0.2r$	1.00^a $(100)^a$	1.00 (1.00)	1.01 (1.00)	1.27 (1.03)	3.01 (4.02)
$z = 0.4r$	1.01 (1.00)	1.00 (1.00)	1.00 (1.00)	1.17 (1.03)	2.12 (4.29)
$z = 0.6r$	1.05 (1.01)	1.06 (1.01)	1.10 (1.01)	1.11 (1.01)	1.05 (1.08)
$z = 0.8r$	1.10 (1.03)	1.18 (1.04)	1.59 (1.08)	1.89 (1.33)	3.63 (2.94)

^{a}The compensated waveforms are derived from the eddy-current affected field responses at these locations, therefore the fwhm should be 1.00 (no mismatching).

coil diameter, respectively (see Table II). Since the mismatching effects in the central imaging volume are relatively small, choice of the eddy-current affected response to derive compensated waveform is not critical. Thus, most of eddy-current af- fected field responses near the central imaging volume can be used for the derivation of the compensated waveform, except those responses near the gradient coil boundary as shown in Table II.

IV. CONCLUSION

The effects of eddy currents in NMR imaging are analyzed from the solution of Maxwell's equations. Their major effects are: i) resolution degradation, ii) misregisteration, iii) loss of signal-to-noise ratio, and iv) phase change. In this paper, degradation of resolution is calculated with the full width at half maximum of the impulse response. The degradation of resolution becomes larger as the pixel position moves farther from the center. The shift of peak position generates a misregisteration problem as well as edge artifacts when interplane image processing is applied. The line broadening introduces signal loss, which can also be an error source of the intensity-based parameter estimations such as T_1, T_2, time-of-flight, diffusion coefficient, and perfusion. The change of phase as a function of spatial coordinate can make a problem associated with the phase-sensitive imaging techniques such as flow, angiography, chemical shift imaging, etc.

The temporal compensation technique is the inverse filtering of the eddy-current affected field response, which is calculated from the diffusion equation. Using an analytic solution, limitation of the temporal compensation technique due to mismatching of the compensated waveform to the spatially variant eddy-current responses is investigated. From the computer simulation, the mismatching effects turned out relatively small in the imaging volume within 60% of the gradient coil diameter. However, the mismatching effects become larger as the position moves closer to the gradient coil boundary (80% of the gradient coil diameter).

REFERENCES

[1] C. B. Ahn and Z. H. Cho, "Analysis of eddy currents in nuclear magnetic resonance imaging," *Magn. Reson. Med.*, vol. 17, pp. 149-163, 1991.

[2] ——, "Analytic solution of eddy currents and its temporal compensation in nuclear magnetic resonance imaging," *Proc. Med. Ima. IV, SPIE*, vol. 1231, pp. 138-149, 1990.

[3] M. A. Morich, D. A. Lampman, W. R. Dannels, and F. T. D. Goldie, "Exact temporal eddy current compensation in magnetic resonance imaging systems," *IEEE Trans. Med. Imag.*, vol. 7, pp. 247-254, 1988.

[4] D. J. Jensen, W. W. Brey, J. L. Delayre, and P. A. Narayana, "Reduction of pulsed gradient settling time in the superconducting magnet of a magnetic resonance instrument," *Med. Phys.*, vol. 14, pp. 859-862, 1987.

[5] P. D. Majors, J. L. Blackley, S. A. Altobelli, A. Caprihan, and E. Fukushima, "Eddy current compensation by direct field detection and digital gradient modification," *J. Magn. Reson.*, vol. 87, pp. 548-553, 1990.

[6] P. Mansfield and B. Chapman, "Active magnetic screening of gradient coils in NMR imaging," *J. Magn. Reson.*, vol. 66, pp. 573-576, 1986.

[7] R. Turner and R. M. Bowley, "Passive screening of switched magnetic field gradients," *J. Phys. E: Instrum.*, vol. 19, pp. 876-879, 1986.

[8] R. L. Stoll, *The Analysis of Eddy Currents*. Oxford, England: Clarendon, 1974, pp. 1-9.

[9] J. A. Tegopoulos and E. E. Kriezis, *Eddy Currents in Linear Conducting Media*. New York: Elsevier, 1985, pp. 165-183.

[10] Z. H. Cho, C. B. Ahn, S. C. Juh, H. K. Lee, R. E. Jacobs, S. Lee, J. H. Yi, and J. M. Jo, "NMR microscopy with 4 μm resolution—Theoretical study and experimental results," *Med. Phys.*, vol. 15, pp. 815-824, 1988.

[11] C. B. Ahn and Z. H. Cho, "A generalized formulation of diffusion effects in μm resolution NMR imaging," *Med. Phys.* vol. 16, pp. 22-28, 1989.

[12] C. B. Ahn, S. Y. Lee, O. Nalcioglu, and Z. H. Cho, "An improved nuclear magnetic resonance diffusion coefficient imaging method using an optimized pulse sequence," *Med. Phys.*, vol. 13, pp. 789-793, 1986.

[13] C. B. Ahn, S. Y. Lee, O. Nalcioglu, and Z. H. Cho, "The effects of random directional distributed flow in nuclear magnetic resonance imaging," *Med. Phys.*, vol. 14, pp. 43-48, 1987.

[14] A. Macovski, "Selective projection imaging: Applications to radiography and NMR," *IEEE Trans. Med. Imag.*, vol. 1, pp. 42-47, 1982.

[15] D. A. Sebok and R. S. Mezrich, "A procedure for creating eddy current field map images," *Book of Abstracts, Soc. Mag. Reson. Med.*, 1988, p. 1079.